Tetrahedron 67 (2011) 1852–1861

Contents lists available at ScienceDirect

Tetrahedron

journal homepage: www.elsevier.com/locate/tet

Multifunctional red phosphorescent bis-cyclometallated iridium complexes based on 2-phenyl-1,2,3-benzotriazole ligand and carbazolyl moieties

Tadas Malinauskas [a], Maryte Daskeviciene [a], Karolis Kazlauskas [b,*], Hai-Ching Su [c], Juozas Vidas Grazulevicius [a], Saulius Jursenas [b], Chung-Chih Wu [d], Vytautas Getautis [a,*]

[a] Faculty of Chemical Technology, Kaunas University of Technology, Radvilenu pl. 19, 50270 Kaunas, Lithuania
[b] Institute of Applied Research, Vilnius University, Sauletekio 9 - III, 10222 Vilnius, Lithuania
[c] Institute of Lighting and Energy Photonics, National Chiao Tung University, Tainan 71150, Taiwan
[d] Department of Electrical Engineering, Graduate Institute of Photonics and Optoelectronics, and Graduate Institute of Electronics Engineering, National Taiwan University, Taipei 106, Taiwan

ARTICLE INFO

Article history:
Received 5 August 2010
Received in revised form 10 December 2010
Accepted 11 January 2011
Available online 15 January 2011

Keywords:
Carbazole
Iridium complex
Phosphorescence
Triazole

ABSTRACT

Multifunctional phosphorescent bis-cyclometallated iridium(III) complexes based on the 2-phenyl-1,2,3-benzotriazole moiety and bearing branched hole-transporting carbazole fragments were synthesized. The isolated compounds were found to be amorphous and expressed very good solubility. Introduction of flexible aliphatic chains of various lengths into the iridium complexes enabled manipulation of their glass transition temperature. The iridium complexes exhibited red phosphorescence emission at 650 nm with the lifetime of 5.7 μs and phosphorescence quantum yields of 0.22 and 0.17 in solution and solid state, respectively, at room temperature. The shielding effect of the carbazolyl moieties on the concentration quenching of phosphorescence of the iridium centers was found to result in the increased excited state lifetime and quantum yield due to the suppressed exciton migration. Non-optimized OLED devices, based on the phosphorescent bis-cyclometallated iridium(III) complex without host material were fabricated and their electroluminescence properties were evaluated.

1. Introduction

Organic light-emitting diodes (OLEDs) are currently attracting a lot of attention owing to their applications in full-color flat-panel displays and solid state lighting.[1] Among the huge variety of organic luminophores available there are phosphorescent ones, which are particularly attractive for electroluminescence applications. In contrast to fluorescent materials they can offer internal quantum efficiencies up to 100% by forcing both singlet and triplet states to emit light.[2] This is achieved by utilizing transition metal–ligand complexes (e.g., iridium(III) complexes), which can overcome the forbidden nature of the transitions from the triplet states due to the strong spin–orbit coupling of the transition metal, giving rise to mixing of the singlet and triplet excited states.[3]

The key-factors limiting application of phosphorescent materials for the emissive layers (EML) in an undiluted form are concentration quenching of emission due to intermolecular interactions and poor charge carrier mobility.[4] To circumvent the problems a doping technique is usually employed in the fabrication of high-performance devices.[5] Dispersing Ir complexes in a host matrix enables spatial separation of the phosphors, resulting in a suppression of concentration quenching and also enhances charge transport. Although the doping technique is effective it can raise additional problems related to phase segregation caused by inhomogeneous distribution of the guest in the host as well as the impossibility to precisely control doping concentration, which is typically well below 10 wt %. These issues are considered to be a serious drawback in the manufacturing of reliable and reproducible commercial devices.

A number of solution-processible phosphorescent polymers with Ir(III) complexes chemically bonded to the side chains, main chain, or end groups has been reported.[6] However, considerable difficulties in purifying polymers severely limit performance of polymer-based devices. Moreover, the triplet energy of the polymer host has to be finely tuned to avoid back energy transfer from the guest molecules giving rise to additional difficulties.[7]

Carbazole derivatives are well-known hole-transporting materials with a tunable triplet energy level. They have been widely used as the host materials of phosphorescent metal complexes for the

* Corresponding authors. Tel.: +370 37 300196; fax: +370 37 300152. (V.G.); tel.: +370 5 2366096; fax: +370 5 2366059 (K.K.); e-mail addresses: karolis.kazlauskas@ff.vu.lt (K. Kazlauskas), vytautas.getautis@ktu.lt (V. Getautis).

0040-4020/$ – see front matter © 2011 Elsevier Ltd. All rights reserved.
doi:10.1016/j.tet.2011.01.026

fabrication of OLEDs.[8] Carbazolyl units were introduced into transition-metal-based complexes to improve charge carrier injection and transport.[9] Formation of such bifunctional molecules via attachment of carbazole-based fragments (acting as a host) to the phosphorescent core (acting as an emissive dopant) is highly desirable for the development of non-doped phosphorescent devices. The main benefits of this design include high triplet energy (>2.9 eV) of the carbazole moieties preventing back energy transfer from the emissive Ir core, shielding effect of the bulky carbazolyl fragments, diminishing intermolecular interactions between emissive Ir cores, and thus, reducing undesired triplet–triplet annihilation[2c, 9c, 10] as well as good charge-transport properties of the bifunctional material provided by the carbazole moieties. The bifunctional molecules capable of performing as a 'self-host' can be used alone for EML for non-doped devices.

For OLEDs to be useful in display applications, true red, green, and blue emissions of sufficient luminescent efficiencies and proper chromaticity are required. To date, there is a greater success in the research of green triplet emitters than red ones. In accordance with the energy-gap law the design and synthesis of efficient red emitters is intrinsically more difficult. The law predicts an increase of the radiationless deactivation rate with a decrease of the emission gap due to the matching of wave functions between the emitting state and highly vibrational levels of the ground electronic state resulting in a fast $T_1 \rightarrow S_0$ internal conversion followed by solvent (or lattice in the solid state) deactivation. Since the quenching mechanism is intrinsic, it causes the main obstacle in achieving red emitters of high efficiency. Hence, many red organic dyes currently in use do not show a good compromise between device efficiency and color purity because of the nature of red emitters.[11]

In the past few years a number of new red emitting iridium complexes for OLEDs have been reported.[12] Various nitrogen-containing heterocycles, such as quinolines, isoquinolines, quinazolines, and quinoxalines have been of special interest in accomplishing red phosphorescent emission. However, 1,2,3-triazoles have been virtually overlooked and only recently few examples have been published.[13] The purpose of the present work is to synthesize red-emitting 1,2,3-triazole-based iridium complexes bearing hole-transporting carbazolyl moieties in order to study their emission properties and to promote them as potential multifunctional 'self-host' phosphorescent materials for non-doped OLED devices.

2. Results and discussion

2.1. Synthesis and characterization

Synthesis of the model iridium complex **4** containing 2-phenyl-1,2,3-benzotriazole moiety was carried out by a four-step synthetic route (Scheme 1).

The first two steps involve preparation of the ligand 5-bis[(2-ethylhexyl)-amino]-2-phenyl-1,2,3-benzotriazole (**2**) by means of cyclization of 2,4-diaminophenylazobenzene, followed by alkylation of 5-amino-2-phenyl-1,2,3-benzotriazole (**1**) with 2-ethylhexyl bromide in the presence of the base KOH. Nonoyama reaction of the synthesized ligand **2** and $IrCl_3 \cdot nH_2O$ in a mixed solvent system of 2-ethoxyethanol and water gave the cyclometalated μ-chloride-bridged Ir(III) dimer. Subsequently, the chloride of the μ-chloride-bridged Ir(III) dimer was substituted by the acetylacetone ligand with the assistance of potassium carbonate in a thoroughly degassed 2-ethoxyethanol at 135 °C.

After successful isolation and identification of the model compound **4** the next step was the synthesis of the bifunctional emitters consisting of hole-transporting carbazole-based outer shell and emissive iridium core. The appropriate ligand 5-bis[3-hydroxy-7-(carbazol-9-yl)-6-(carbazol-9-methyl)-5-oxa-1-heptylamino]-2-phenyl-1,2,3-benzotriazole (**5**) was prepared by the reaction of **1** with 1,3-di(carbazol-9-yl)-2-propanol glycidyl ether in the melt phase at 160 °C (Scheme 2). Hydroxyl groups, present in the molecule, could be easily alkylated with various alkyl halides; thus, providing a convenient way to control the glass transition temperature. To demonstrate this possibility the carbazole-containing ligand **6** with blocked hydroxyl groups was obtained by alkylating compound **5** with 1-iodoethane in the presence of KOH. μ-Chloride-bridged dimers **7a**,**b** and iridium complexes **8a**,**b** (Scheme 3), possessing carbazole-based hole-transporting fragments, were obtained by the same synthetic procedure as used for the preparation of compounds **3** and **4**.

All three cyclometalated complexes **4**, **8a**,**b** are readily soluble in common organic solvents. Their good solubility can be attributed to the flexible aliphatic fragments.

Complexes **8a**,**b** were studied by DSC. These investigations revealed that **8a** and **8b** are amorphous, and the glass transition occurs at 146 °C and 117 °C, respectively. Introduction of additional flexible aliphatic chains of various lengths and elimination of

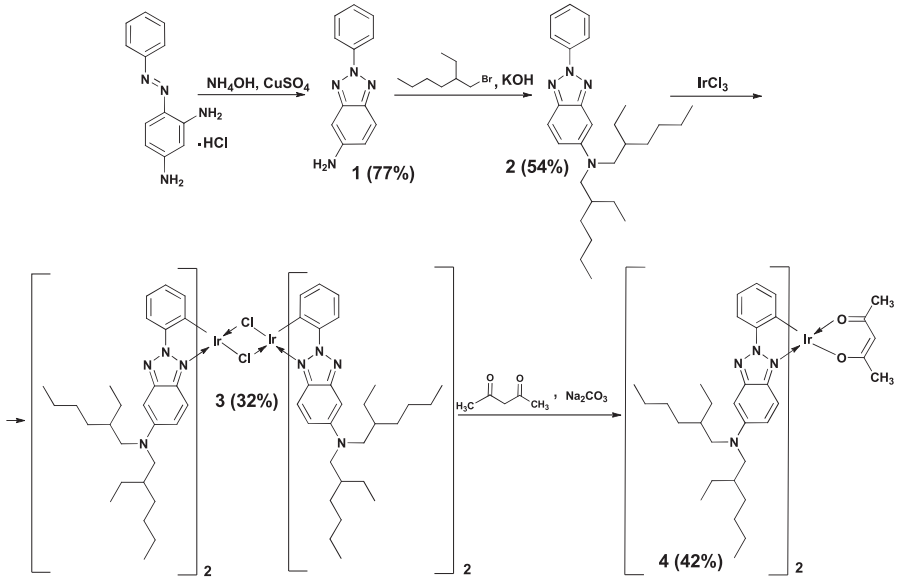

Scheme 1. Synthesis of 1,2,3-benzotriazole-based iridium complex **4**.

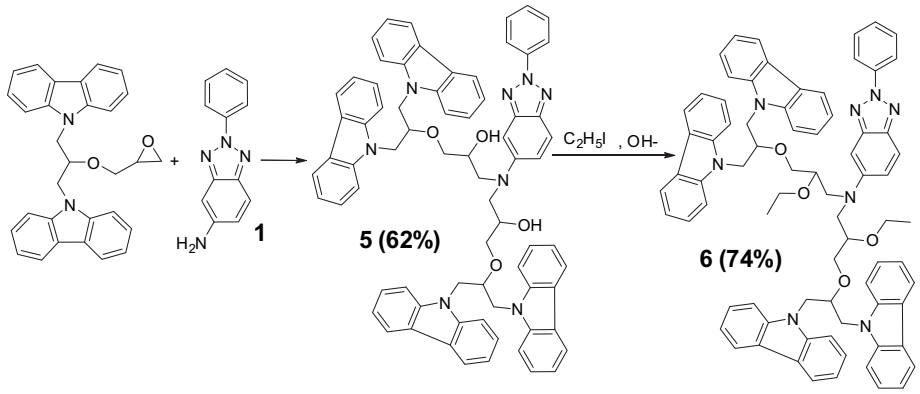

Scheme 2. Synthesis of ligands **5**, **6**.

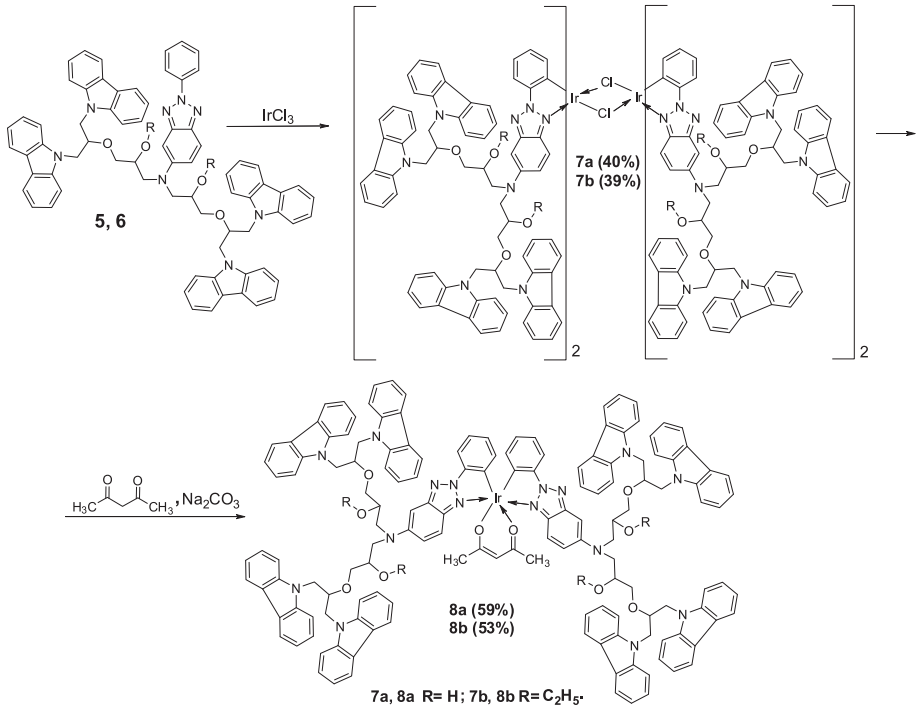

Scheme 3. Synthesis of iridium complexes **8a**,**8b**.

hydroxyl groups allows successful manipulation of the glass transition temperature. In this case T_g of the ethyl-substituted compound **8b** is by 29 °C lower as compared with **8a**. The results of thermal studies indicate that the glasses of the synthesized organometallic compounds are morphologically stable. They show only glass transitions in repeated differential scanning calorimetry runs.

2.2. Photophysical and electrochemical properties

The absorption spectra of THF solutions of the iridium complexes **4**, **8a**, **8b** and the corresponding ligands **2**, **5**, **6** are displayed in Fig. 1. The details of the optical properties of the compounds studied are summarized in Table 1.

By comparing features observed in the spectra of the ligands and iridium complexes we can attribute the band centered at 390 nm to $\pi\rightarrow\pi^*$ transition of the 2-phenyl-1,2,3-benzotriazole ligand. The bands located in the region of 300–350 nm and exhibiting well-resolved vibronic structure observed in the spectra of the carbazolyl groups-containing ligands **5**, **6** and complexes **8a**, **8b** are associated to $\pi\rightarrow\pi^*$ and $n\rightarrow\pi^*$ transitions of the carbazolyl fragments. An

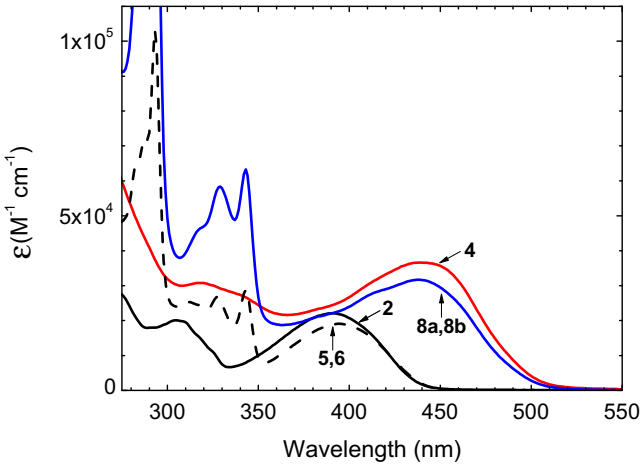

Fig. 1. Absorption spectra of the dilute THF solutions (10^{-4} M) of bis-cyclometallated iridium complexes **4**, **8a**, **8b** and corresponding ligands **2**, **5**, **6**.

Table 1
Optical characteristics of the bis-cyclometallated iridium complexes **4**, **8a**, **8b** and the corresponding ligands **2**, **5**, **6**

Entry	Solutions				Films		
	λ^{abs}_{max}/nm[a] (log ϵ, $M^{-1}\times cm^{-1}$)	λ^{PL}_{max}/nm [b]	η	τ	λ^{PL}_{max}/nm	η	τ
2	250 (4.58), 391 (4.34)	449	0.42	3.9 ns	495	0.02	Non-exp. [c]
4	257 (4.92), 440 (4.56)	619, 669	0.16	5.7 μs	625, 672	0.01	Non-exp. [c]
5	293 (5.01), 343 (4.46), 394 (4.28)	450	0.42	3.9 ns	470	0.23	Non-exp. [c]
6	293 (5.01), 343 (4.46), 394 (4.28)	450	0.42	3.9 ns	470	0.23	Non-exp. [c]
8a	293 (5.25), 343 (4.80), 439 (4.50)	619, 669	0.22	5.7 μs	625, 672	0.17	Non-exp. [c]
8b	293 (5.25), 343 (4.80), 439 (4.50)	619, 669	0.22	5.7 μs	625, 672	0.17	Non-exp. [c]

[a] Absorption spectra measured in 10^{-4} M THF solution.
[b] PL spectra measured in 10^{-5} M toluene solution. Excitation wavelength 366 nm.
[c] Non-exponential PL decay.

appearance of the long-wavelength absorption band at 440 nm in the spectra of all the iridium complexes studied and the absence of this band in the spectra of the ligands indicate the band originates from the cyclometallation process. In close analogy to the absorption spectra of the iridium complex based on phenyltriazole-quinoline ligand[13c] the long-wavelength absorption band can involve transitions to both singlet and triplet metal-to-ligand charge transfer (MLCT) states, though contribution of ligand centered (LC) transitions is also possible.

Fig. 2 illustrates PL spectra of the dilute solutions and solid films of bis-cyclometallated iridium complexes **4**, **8a**, **8b** and of the corresponding ligands **2**, **5**, **6**. The PL spectra of the 2-phenyl-1,2,3-benzotriazole ligand **2** and the analogous carbazolyl-containing ligands **5**, **6** are identical in solution and have a maximum at 450 nm. Moreover, the ligands **2** and **5**, **6** in the solution exhibit the same PL quantum yield (η=0.42) despite exciting to either phenyl-benzotriazole or both phenyl-benzotriazole and carbazolyl groups. This indicates negligible influence of the carbazolyl fragments on the emission properties of the ligands in solution. In contrast to this, carbazolyl fragments are found to have a crucial impact on the ligand PL in the solid state. The PL spectrum of the film of the ligand **2** is red shifted by 50 nm and significantly broadened as compared to that of the solution. Additionally, a 20-fold decrease in PL quantum yield of the film is obtained. However, the PL of ligands **5**, **6** in films exhibited twice as small red shift, no spectral broadening

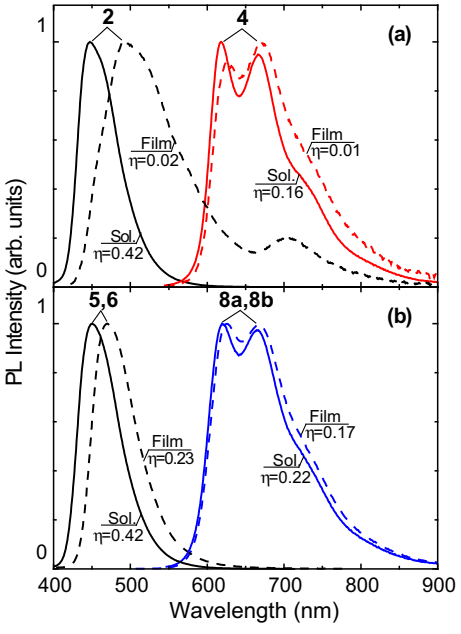

Fig. 2. PL spectra of degassed 10^{-5} M toluene solutions (solid lines) and films (dashed lines) of the iridium complexes **4**, **8a**, **8b** and the corresponding ligands **2**, **5**, **6**. (a) The spectra of the compounds containing no carbazolyl groups, (b) containing carbazolyl groups. PL quantum yield (η) values are indicated.

and only a twofold decrease in the quantum yield as compared to that in the solutions. Obviously, the small changes in the PL properties of the solutions and films of the compounds **5**, **6** are provoked by carbazolyl moieties, which separate fluorescent 2-phenyl-1,2,3-benzotriazole fragments in a solid state by preventing excitation transfer, and thus, concentration quenching of the emission.[9a] Ligand **2**, containing no carbazolyl moieties, is subjected to a considerable concentration quenching in the solid state, which is also evidenced by the appearance of an additional band at 710 nm attributed to an excimer state formation.

A similar effect of the carbazolyl moieties on the PL properties is also observed for the iridium complexes **4**, **8a**, **8b** (Fig. 2). The iridium complexes in a solution and solid state feature single PL band centered at 650 nm with well-resolved vibronic structure, which is more supportive of LC-type transitions than of MLCT. Pure MLCT states are known to exhibit broad and structureless emission bands caused by CT character.

The phosphorescence origin of the band was verified by the microsecond-time-scale decay and an efficient quenching of the emission by molecular oxygen. Commission Internationale de l'Eclairage (CIE) chromaticity coordinates (x, y) of the complexes were found to be (0.61, 0.33) corresponding to the red color (Fig. 3). The spectral shapes and positions of the phosphorescence bands of the iridium complexes **4**, **8a**, **8b** measured either in solution or solid state show only insignificant differences, however, essential differences are revealed in the PL quantum yield. In the case of the iridium complex **4** containing no carbazolyl groups, a considerable drop in the quantum yield from η=0.16 (in the solution) to η=0.01 (in the film) was observed, whereas only negligible reduction of the quantum yield from

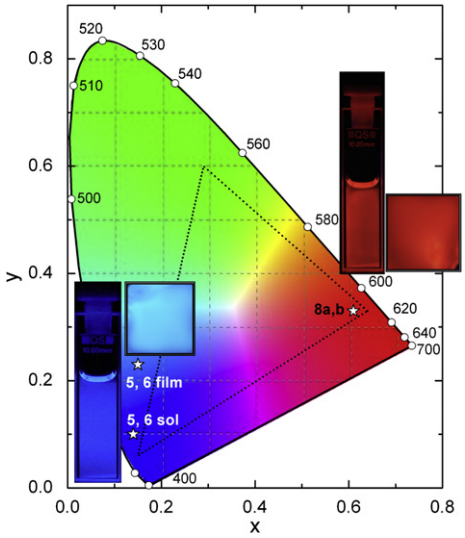

Fig. 3. CIE 1931 *xy* chromaticity diagram with the coordinates of the iridium complexes **8a**, **8b** and the corresponding ligands **5**, **6**. The vertices of the triangle indicate coordinates of the RGB primaries specified by the HDTV standard.

η=0.22 (in the solution) to η=0.17 (in the film) was obtained for the carbazolyl-containing iridium complexes **8a**, **8b**. This is a relatively good result, as compounds with phosphorescence maxima around 640–660 nm have been reported to reach the quantum yields of approximately 0.10–0.30 in the solution.[5a,14] Again, as in the previous case of the ligands, we attribute this effect to increased intermolecular separation induced by the presence of the bulky carbazolyl moieties, which in turn, suppress concentration quenching of the phosphorescence emission from iridium cores.

Interestingly enough, electron donating tertiary amino group, present in the 1,2,3-benzotriazole segment of the ligand in the Ir complexes **4**, **8a**, **8b**, has a much more profound effect on the emission wavelength than electron donating moiety attached to the phenyl ring of the same ligand.[13b,d] Namely, iridium complexes reported in the literature, with various electron donating substituents at *para*-position of the phenyl ring, demonstrate orange PL emission centered around 590–600 nm, while **4**, **8a**, **8b** are red emitting compounds.

To further support the shielding effect of the carbazolyl moieties on the concentration quenching, PL lifetime measurements of the ligands **2**, **5**, **6** (Fig. 4) and the bis-cyclometallated iridium complexes **4**, **8a**, **8b** (Fig. 5) were performed.

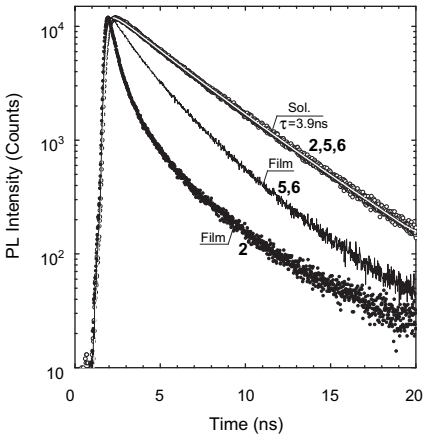

Fig. 4. PL transients of 10^{-5} M toluene solutions and films of the ligands **2**, **5**, **6** measured at the spectral maximum. Line indicates single exponential fit to the experimental data.

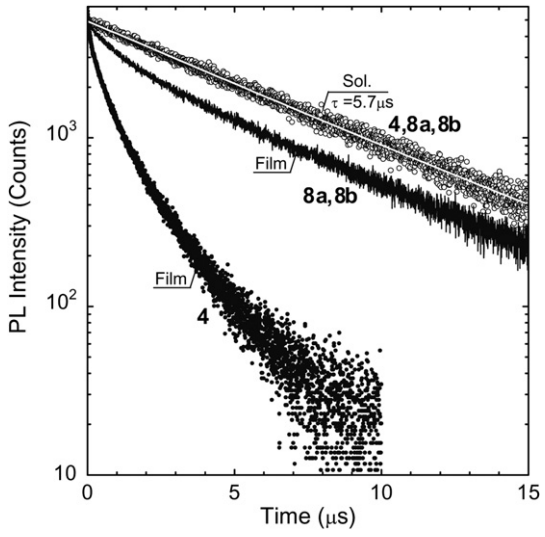

Fig. 5. PL transients of the degassed 10^{-5} M toluene solutions and encapsulated films of iridium complexes **4**, **8a**, **8b** measured at the spectral maximum. The line indicates single exponential fit to the experimental data.

The PL transients of all the ligands in a dilute solution exhibited single exponential decay with a lifetime of τ=3.9 ns. Somewhat faster and non-exponential decay was observed for the films of carbazolyl-containing ligands **5**, **6**, whereas for the ligand **2** containing no carbazolyl groups the decay became even more rapid indicating substantially shortened excited state lifetime. The pronounced non-exponential fast decay in a solid state usually signifies migration-enhanced exciton quenching, which in the case of the ligand **2** is obviously caused by enhanced intermolecular interaction. The slower PL decay observed for the films of the ligands **5**, **6** points out the importance of the carbazolyl groups in strongly diminishing the intermolecular interaction.

Even more pronounced influence of the carbazolyl moieties on the PL decay was observed for the phosphorescent iridium complexes **4**, **8a**, **8b**. In dilute solutions all the complexes exhibited single exponential decays with the lifetime of τ=5.7 μs. This rather long microsecond lifetime and roughly five times longer radiative lifetime (τ/η) show that iridium character in the emissive state is not significant again pointing out the LC-type transitions to be prevalent over MLCT. In the solid state, the PL transient of the carbazolyl groups-containing iridium complexes **8a**, **8b** was only slightly faster as that in a solution in the initial stage; however, it became identical to that in the solution in the later stage. In sharp contrast to this, the PL decay of the film of iridium complex **4** exhibited extremely rapid decay during all the time-stages indicating considerably reduced excited state lifetime. Evidently, the absence of carbazolyl groups in the iridium complex **4** resulted in a closer intermolecular distance (increased intermolecular interaction) of phosphorescent Ir centers, and consequently, to exciton migration-induced lifetime decrease. Meanwhile the bulky carbazolyl groups in the complexes **8a**, **8b** effectively increased separation of the Ir centers, hereby substantially increasing excited state lifetime by suppressing concentration quenching.

The ionization energy (E_I) was measured by the electron photoemission in air method. The $I^{0.5}=f(h\nu)$ dependencies are shown in Fig. 6. Usually the dependence of the photocurrent on incident light quanta energy is well described by linear relationship between $I^{0.5}$ and $h\nu$ near the threshold. The linear part of this dependence was extrapolated to the $h\nu$ axis and E_I value was determined as the photon energy at the interception point. The measured ionization energies vary in the range from 5.35 eV to 5.67 eV (Table 2). These results show that the formation of the Ir(III) complexes decreases the E_I, as compared with that of the corresponding ligands.

To elucidate the energetic conditions for energy and electron transfer in dilute solutions the HOMO values were also determined using cyclic voltammetry. These E_{HOMO} values do not represent any

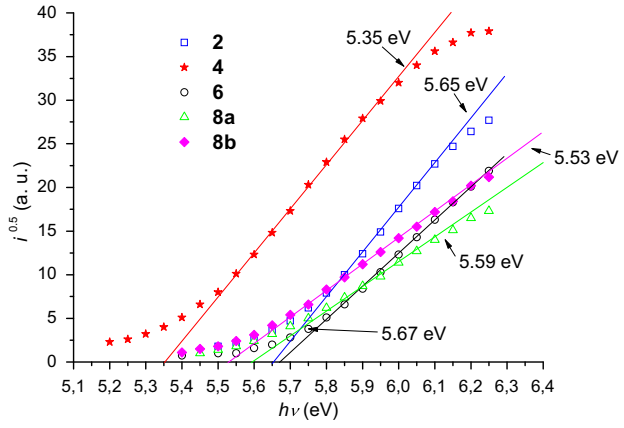

Fig. 6. Photoemission in air spectra of the iridium complexes **4**, **8a**, **8b** and the corresponding ligands **2**, **6**.

Table 2
HOMO, ionization energy and electrochemical properties of **2**, **4**–**6**, **8a**,**b**[a]

Entry	E_{onset} versus Fc/V	E_I/eV[b]	E_{HOMO}/eV[c]
2	0.40	5.65	−5.20
4	0.33	5.35	−5.13
5	0.39	5.67	−5.19
6	0.38	5.64	−5.18
8a	0.34	5.59	−5.14
8b	0.34	5.53	−5.14

[a] The measurements were carried out at a glassy carbon electrode in dichloromethane solutions containing 0.1 M tetrabutylammonium hexafluorophosphate as electrolyte and $Ag/AgNO_3$ as the reference electrode. Each measurement was calibrated with ferrocene (Fc).
[b] Ionization energy was measured by the photoemission in air method from films.
[c] E_{HOMO}=4.8+(E_{onset} vs Fc).

absolute solid state or gas-phase ionization energies, but can be used to compare different compounds relative to one another. The cyclic voltammograms of the synthesized compounds in dichloromethane solutions show irreversible oxidation in the case of the ligands, quasi-reversible for the Ir(III) complexes and no reduction waves (Fig. 7). The electrochemical data is summarized in Table 2.

The ligands **2**, **5**, **6** show oxidation peaks corresponding to approximately 0.40 V versus Fc, which results in a E_{HOMO} value of about −5.20 eV (on the basis of the E_{HOMO} energy level of ferrocene as 4.8 eV). The complexes **4**, **8a**, **8b** exhibit an oxidation at around 0.34 V versus Fc. This gives E_{HOMO} value of −5.14 eV. The results of CV measurements indicate that E_{HOMO} energy levels increase slightly in the case of the cyclometallated iridium derivatives, if compared with the corresponding ligands.

To evaluate the electroluminescent (EL) properties of the developed iridium complexes, several OLED devices were fabricated using **8a**. The devices were fabricated on glass substrates with the typical structure of multiple organic layers sandwiched between the bottom ITO anode and the top metal cathode (Al) (Fig. 8). The device structure used for device 1 was ITO/**8a** (100 nm)/Ca (20 nm)/Al (150 nm). For device 2, the device structure was ITO/**8a** (100 nm)/BCP (50 nm)/LiF (0.5 nm)/Al (150 nm), where 2,9-dimethyl-4,7-diphenyl-1,10-phenanthroline (BCP) and LiF were used as electron-transport and electron-injection layers, respectively. The device structure used for device 3 was ITO/PEDOT:PSS (30 nm)/**8a** (100 nm)/BCP (50 nm)/LiF (0.5 nm)/Al (150 nm), where PEDOT:PSS was used as hole-injection layer.

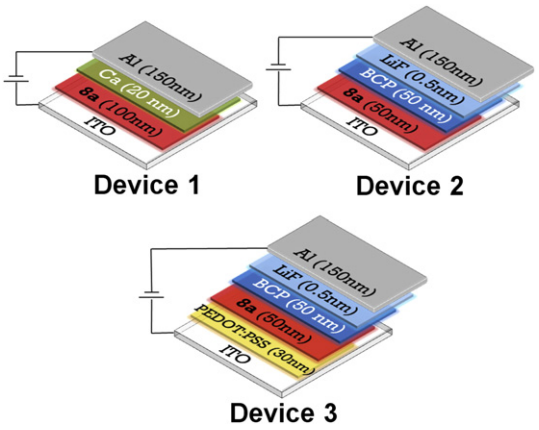

Fig. 8. The general structure for the OLED devices **1**–**3**.

EL characteristics of the non-optimized OLED devices 1–3 are summarized in Table 3. Current density, brightness, and external

Table 3
EL characteristics of the non-optimized devices **1**–**3**

Device	λ^{EL}_{max}/nm	V_{on}/V[a]	V_{max}/V[b]	B_{max}/cd m^{-2}[c]	η_{max}/%[d]
1	628	14.7	22	109	0.11
2	632	10.7	21	587	1.78
3	629	8.2	16	767	1.81

[a] Turn-on voltage at brightness ~1 cd/m^2.
[b] Voltage at the maximum brightness.
[c] The maximum brightness.
[d] Maximal external quantum efficiency.

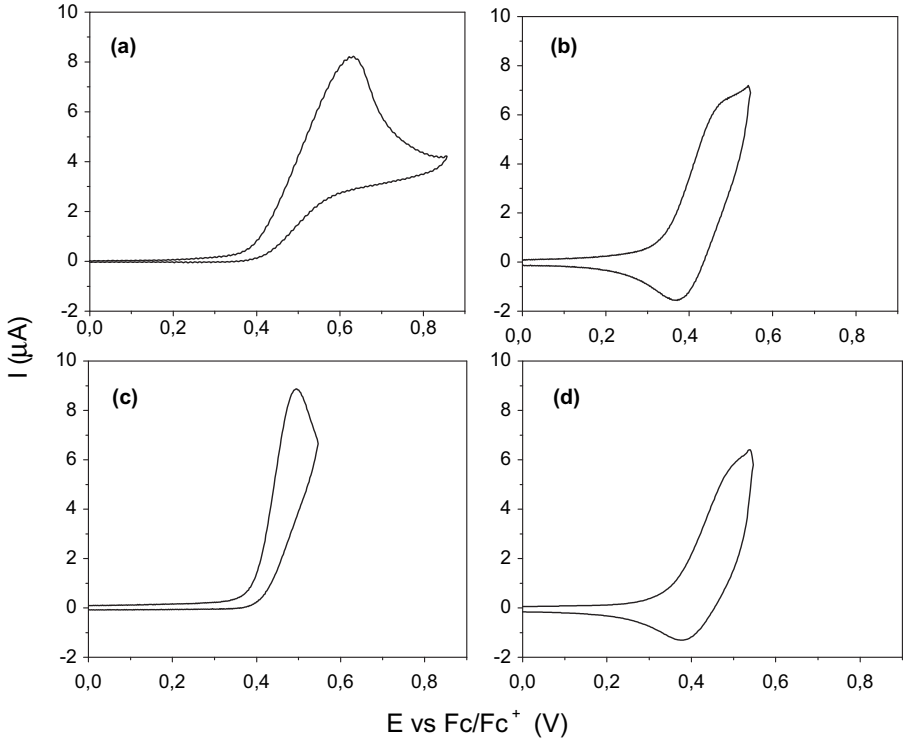

Fig. 7. Cyclic voltammograms of **2** (a), **4** (b), **6** (c), **8b** (d) (scan rate=50 mV s^{-1}) in argon-purged dichloromethane solutions.

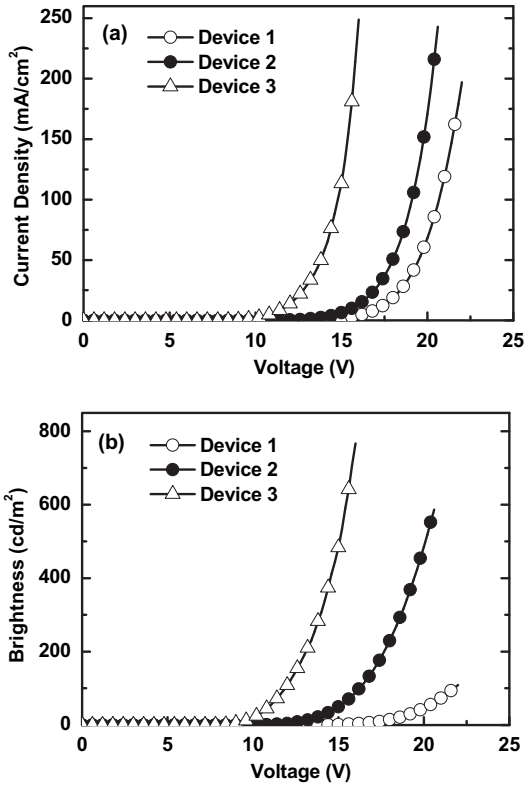

Fig. 9. (a) Current density versus applied voltage, (b) brightness versus applied voltage for non-optimized OLED devices based on **8a**.

quantum efficiency versus applied voltage for OLED devices 1–3 are shown in Figs. 9 (a),(b), and 10, respectively.

Single-layered device 1 exhibited a high turn-on voltage, perhaps due to poor carrier injection, which also resulted in a low device efficiency. Addition of electron-injection and electron-transport layers in device 2 reduced the turn-on voltage and also improved the device efficiency. Further improvement of turn-on voltage and device efficiency was achieved by adding a hole-injection layer, PEDOT:PSS (Device 3).

The maximal external quantum efficiency of OLED device based on **8a** was 1.81%. EL spectra of devices 1–3 are shown in Fig. 11.

The PL spectrum of **8a** neat film is also shown for comparison. EL spectra are basically similar to PL spectra, indicating similar emission mechanisms.

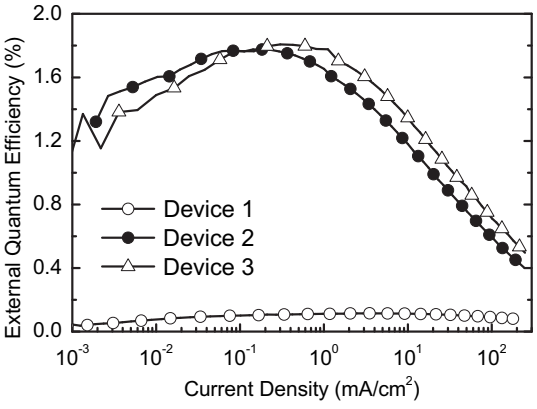

Fig. 10. External quantum efficiency versus current density for non-optimized OLED devices based on **8a**.

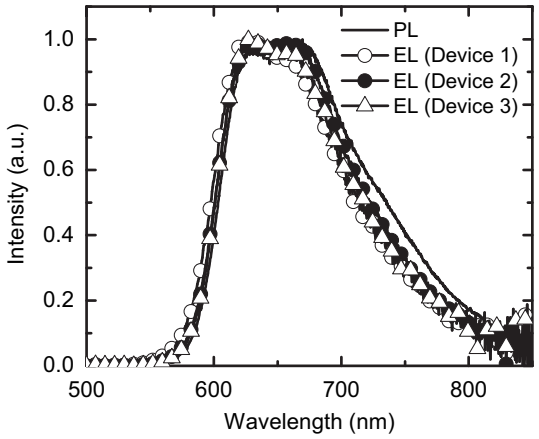

Fig. 11. PL and EL spectra of iridium complex **8a**.

3. Conclusion

Bifunctional phosphorescent bis-cyclometallated iridium(III) complexes based on the 2-phenyl-1,2,3-benzotriazole and branched hole-transporting carbazole moieties were designed. The isolated amorphous compounds were found to express good solubility in common organic solvents, and their glass transition temperatures could be successfully manipulated by introduction of additional flexible aliphatic chains of various lengths. The reduction of T_g by 29 °C with the addition of relatively short ethyl groups was achieved. The bifunctional iridium complexes were found to exhibit red phosphorescence at 650 nm with the CIE chromaticity coordinates of (0.61, 0.33), the phosphorescence lifetime of 5.7 μs and the quantum yields of 0.22 and 0.17 in the solution and solid state, respectively. This is a good result, since the iridium complexes with phosphorescence maxima around 630–660 nm have been reported to reach the quantum yields of approximately 0.10–0.30 in the solution. The electron donating tertiary amine group present in the 1,2,3-benzotriazole segment of the Ir complexes was found to have a more profound effect on the emission wavelength than any other electron donating moiety attached to the phenyl ring of the triazole molecule reported in the literature. The role of branched carbazolyl moieties as intermolecular spacers, which effectively increase separation of the phosphorescent Ir centers, and thus, considerably increase excited state lifetime by suppressing concentration quenching was elucidated. Non-optimized phosphorescent OLEDs, based on the bis-cyclometallated iridium(III) complex without host material, were demonstrated.

4. Experimental section

4.1. Materials

All chemicals were purchased from Aldrich and used as received without further purification. The details of the synthesis of the 1,3-bis(carbazol-9-yl)-2-propanol glycidyl ether are described in Ref. 15.

4.2. General experiments

The 1D and 2D ^{1}H NMR spectra were recorded on a Varian Unity Inova (300 MHz) spectrometer at room temperature. All the data are given as chemical shifts in δ (ppm), $(CH_3)_4Si$ (TMS, 0 ppm) was used as an internal standard. ^{13}C NMR spectra were recorded at 75 MHz and were referenced to $CDCl_3$ or DMSO-d_6. The course of the reactions were monitored by TLC on ALUGRAM SIL G/UV254 plates and developed with I_2 or UV light. Silica gel (grade 62, 60–200 mesh, 150 Å, Aldrich) was used for column

chromatography. Elemental analysis was performed with an Exeter Analytical CE-440 Elemental. IR-spectroscopy was performed on a Perkin Elmer Spectrum BX II FT-IR System, using KBr pellets. Melting points were determined using Electrothermal Mel-Temp melting point apparatus. MS were recorded on an Agilent 110 (series MS with VL) apparatus. The differential scanning calorimetry (DSC) measurements were carried out on a Mettler DSC 30 calorimeter at a scan rate of 10 K/min.

Absorption spectra of the compound THF solutions (10^{-4} M) placed in a 1 mm path length microcell were recorded on a Perkin Elmer Lambda 35 UV–vis spectrometer. Photoluminescence (PL) of the sample toluene solutions (10^{-5} M) and thin films were excited by 366 nm-wavelength light-emitting diode (Nichia NSHU590-B) and measured using back-thinned CCD spectrometer PMA-11 (Hamamatsu). The solutions were degassed to remove dissolved oxygen, and thus, avoid quenching of the radiative decay from the triplet states. The films were prepared from 5×10^{-3} M toluene solutions on the glass substrates by drop-casting under nitrogen atmosphere in the glove box (MBraun UNIlab). Prior to removal of the films out of the glove box they were encapsulated by using an epoxy resin as a sealant and another glass plate on top. The PL quantum yield of the degassed solutions was estimated by comparing wavelength-integrated PL intensity of the solution with that of the reference. Quinine sulfate dissolved in 0.1 M H_2SO_4 with η=53±2.3% at an excitation wavelength of 366 nm has been used as a reference.[16] Optical densities of the reference and the sample solutions were ensured to be below 0.05 to avoid reabsorption effects. Estimated quantum yield was verified by using an alternative method utilizing an integrating sphere.[17] The integrated sphere method was also employed in the quantum yield estimations of the encapsulated films.

PL lifetimes of the sample solutions and thin films were determined using time-correlated single photon counting system (PicoQuant PicoHarp 300). Pulsed excitation with the pulse duration of 70 ps, the emission wavelength of 375 nm and the repetition rate of up to 1 MHz was provided by diode laser.

4.2.1. Electrochemical measurements. Cyclic voltammetry measurements were carried out by a three-electrode assembly cell from Bio-Logic SAS and a micro-AUTOLAB Type III potentiostat–galvanostat. The measurements were carried out with a glassy carbon electrode in dichloromethane solutions containing 0.1 M tetrabutylammonium hexafluorophosphate as electrolyte, $Ag/AgNO_3$ as the reference electrode and a Pt wire counter electrode.

4.2.2. Ionization energy measurements. The ionization energy of the sample films was estimated by performing electron photoemission spectroscopy in air.[18] The samples for the ionization energy measurement were prepared by dissolving materials in THF and were coated on Al plates pre-coated with ~0.5 μm thick methylmethacrylate and methacrylic acid copolymer adhesive layer. The thickness of the transporting material layer was 0.5–1 μm. Usually the photoemission experiments are carried out in vacuum, and high vacuum is one of the main requirements for these measurements. If the vacuum is not high enough, sample surface oxidation and gas adsorption are influencing the measurement results. In our case, however, the organic materials investigated are stable enough to oxygen and the measurements may be carried out in air.

The samples were illuminated with monochromatic light from the quartz monochromator with a deuterium lamp. The power of the incident light beam was $(2–5)\times10^{-8}$ W. The negative voltage of −300 V was supplied to the sample substrate. The counter-electrode with the 4.5×15 mm^2 slit for illumination was placed at an 8 mm distance from the sample surface. The counter-electrode was connected to the input of the BK2-16 type electrometer, working in the open input regime, for the photocurrent measurement. The 10^{-15}–10^{-12} A photocurrent was flowing in the circuit under illumination. The photocurrent I is strongly dependent on the incident light photon energy $h\nu$. The $I^{0.5}=f(h\nu)$ dependence was plotted. Usually the dependence of the photocurrent on incident light quanta energy is well described by the linear relationship between $I^{0.5}$ and $h\nu$ near the threshold. The linear part of this dependence was extrapolated to the $h\nu$ axis and the E_I value was determined as the photon energy at the interception point.

4.3. Device fabrication

OLEDs were fabricated on indium tin oxide (ITO)-coated glass substrates with multiple organic layers sandwiched between the transparent bottom ITO anode and the top metal cathode. The poly (3,4-ethylenedioxythiophene):poly(styrene sulfonate) (PEDOT:PSS) and **8a** layers were prepared by spin coating, whereas other organic layers were fabricated by vacuum evaporation in a vacuum chamber with a base pressure of ~10^{-6} Torr. The deposition rate of organic layers was kept at approximately 0.2 nm/s. The active area of the device was 1×1 mm^2, as defined by the shadow mask for cathode deposition. The I–V–L characteristics of devices were measured by using an Agilent 4155B semiconductor parameter analyzer and a Si photodiode calibrated with Photo Research PR-650 spectroradiometer. Electroluminescent (EL) spectra of devices were collected by a calibrated CCD spectrograph.

4.4. Synthesis

*4.4.1. 5-Amino-2-phenyl-1,2,3-benzotriazole (**1**).* 2,4-Diaminophenylazobenzene hydrochloride (10.5 g, 0.0422 mol), $CuSO_4\cdot5H_2O$ (62.5 g, 0.25 mol), 25% solution of NH_4OH (100 mL, 0.78 mol) were refluxed in 350 mL of 50% ethanol solution in water for 4 h (TLC: diethyl ether/*n*-hexane, 2:1 v/v) and cooled down in the ice bath. The crystals were filtered, washed with water several times and dried to afford **1** (6.8 g, 77%) as brown needle crystals, mp: 180–182 °C (ethyl acetate); [found: C, 68.43; H, 4.68; N, 26.72. $C_{12}H_{10}N_4$ requires C, 68.56; H, 4.79; N, 26.65%]; R_f (diethyl ether/*n*-hexane, 2:1 v/v) 0.35; ν_{max} (KBr) 3416, 3325; 3060 cm^{-1}; δ_H (300 MHz, DMSO-d_6) 8.20 (d, J=8.19 Hz, 2H, 2-H, 6-H of 1-subst Ph), 7.90–7.30 (m, 4H, 7-H_{Ht}, 3-H, 5-H of 1-subst Ph, 4-H of 1-subst Ph), 7.01 (d, J=7.0 Hz, 1H, 6-H_{Ht}), 6.71 (s, 1H, 4-H_{Ht}), 5.68 (s, 2H, NH_2); δ_C (75 MHz, DMSO-d_6) 92.3, 118.4, 119.3, 122.8, 128.1, 129.7, 139.6, 139.8, 146.7, 148.4; MS (APCI$^+$, 20 V), m/z: 211 ([M+H]$^+$).

*4.4.2. 5-Bis[(2-ethylhexyl)]amino-2-phenyl-1,2,3-benzotriazole (**2**).* 5-Amino-2-phenyl-1,2,3-benzotriazole (8.0 g, 0.0382 mol), Na_2SO_4 (2.7 g, 0.0191 mol), and powdered 85% potassium hydroxide (4.6 g, 0.115 mol) were refluxed at 160 °C in 40 mL of 2-ethylhexyl bromide for 24 h (TLC: acetone/*n*-hexane, 1:49 v/v). The mixture was cooled to room temperature and filtered off. The organic part was treated with ethyl acetate and washed with distilled water until the wash water was neutral. The organic layer was dried over anhydrous Na_2SO_4, filtered, and solvents were removed. The obtained residue was dissolved in 2-ethylhexyl bromide (40 mL), Na_2SO_4 (2.7 g, 0.0191 mol), and powdered 85% potassium hydroxide (4.6 g, 0.115 mol) was added and all processes were repeated. The residue was purified by column chromatography using acetone/*n*-hexane (1:49 v/v) as eluent to obtain **2** (8.97 g, 54%) as brown-green oil; [found: C, 77.42; H, 9.68; N, 12.90. $C_{28}H_{42}N_4$ requires C, 77.37; H, 9.74; N, 12.89%]; R_f (acetone/*n*-hexane, 1:49 v/v) 0.74; ν_{max} (KBr) 3048; 2928, 2869 cm^{-1}; δ_H (300 MHz, $CDCl_3$) 8.27 (d, J=7.5 Hz, 2H, 2-H, 6-H of 1-subst Ph), 7.72 (d, J=9.5 Hz, 1H, 7-H_{Ht}), 7.51 (t, J=7.5 Hz, 2H, 3-H, 5-H of 1-subst Ph), 7.37 (t, J=7.5 Hz, 1H, 4-H of 1-subst Ph), 7.14 (dd, J=9.5 Hz, J=2.2 Hz, 1H, 6-H_{Ht}), 6.79 (d, J=2.2 Hz, 1H, 4-H_{Ht}), 3.36–3.20 (m, 4H, NCH_2), 1.93–1.72 (m, 2H, CH), 1.44–1.13 (m, 16H, CH_2), 0.97–0.76 (m, 12H, CH_3); δ_C (75 MHz,

$CDCl_3$) 148.0, 147.4, 140.7, 139.9, 129.5, 128.0, 121.0, 120.1, 118.3, 94.1, 57.2, 37.1, 30.9, 28.9, 24.1, 23.4, 14.3, 10.9; MS (APCI$^+$, 20 V), *m*/*z*: 435 ([M+H]$^+$).

*4.4.3. Tetrakis{5-bis[(2-ethylhexyl)]amino-2-phenyl-1,2,3-benzotriazole-N,C$^{2'}$}(μ-dichloro)diiridium (**3**).* Iridium trichloride hydrate (0.4 g, 1.33 mmol) and 5-bis[(2-ethylhexyl)amino]-2-phenyl-1,2,3-benzotriazole (**2**) (1.7 g, 4.01 mmol) were dissolved in the mixture of 2-ethoxyethanol (10 mL) and water (5 mL). The mixture was refluxed under argon atmosphere for 24 h, and cooled down to the room temperature (TLC: acetone/*n*-hexane, 1:4 v/v). Obtained solution was extracted with chloroform and distilled water several times. The organic layer was dried over anhydrous $MgSO_4$, filtered, and solvents were evaporated. The residue was purified by column chromatography using *n*-hexane and acetone/*n*-hexane (3:22 v/v) as eluent to obtain **3** (0.95 g, 32%) as an orange solid.

*4.4.4. Iridium(III)-bis{5-bis[(2-ethylhexyl)]amino-2-phenyl-1,2,3-benzotriazolato-N,C$^{2'}$}acetylacetonate (**4**).* The μ-chloride-bridged dimer **3** (0.91 g, 0.415 mmol), 2,4-pentanedione (0.125 g, 1.25 mmol) and sodium carbonate (0.44 g, 4.15 mmol) were refluxed in 8 mL of degassed 2-ethoxyethanol under argon atmosphere for 1 h. After termination of the reaction (TLC: acetone/*n*-hexane, 3:97 v/v) obtained solution was extracted with chloroform and distilled water several times. The organic layer was dried over anhydrous $MgSO_4$, filtered, and solvents were evaporated. The residue was purified by column chromatography using *n*-hexane and acetone/*n*-hexane (1:99 v/v) as eluent to obtain **4** (0.4 g, 42%) as a brown solid; [found: C, 63.29; H, 7.68; N, 9.60. $C_{61}H_{89}IrN_8O_2$ requires C, 63.24; H, 7.74; N, 9.67%]; R_f (acetone/*n*-hexane, 3:97 v/v) 0.53; ν_{max} (KBr) 3050, 2927, 2871, 1698 cm^{-1}; δ_H (300 MHz, $CDCl_3$) 7.82–7.71 (m, 3H, 6-H of 1-subst Ph, 7-H_{Ht} of one tetrazole fragment), 7.50 (dd, *J*=9.5 Hz, *J*=3.8 Hz, 1H, 7-H_{Ht} of other tetrazole fragment), 7.20 (d, *J*=9.5 Hz, 1H, 6-H_{Ht} of one tetrazole fragment), 7.14–7.06 (m, 1H, 6-H_{Ht} of other tetrazole fragment), 6.97–6.84 (m, 3H, 5-H of 1-subst Ph, 4-H_{Ht} of one tetrazole fragment), 6.78–6.73 (m, 1H, 4-H_{Ht} of other tetrazole fragment), 6.70–6.59 (m, 2H, 4-H of 1-subst Ph), 6.34–6.22 (m, 1H, 3-H of 1-subst Ph, of one ligand fragment), 6.19–6.08 (m, 1H, 3-H of 1-subst Ph, of other ligand fragment), 5.25 (s, 1H, CCHC), 3.50–3.11 (m, 8H, NCH_2), 1.95–1.70 (m, 10H, CH, CCH_3), 1.45–1.10 (m, 32H, CH_2), 0.97–0.76 (m, 24H, CH_3); δ_C (75 MHz, $CDCl_3$) 186.0, 185.5, 150.53, 150.48, 146.65, 146.62, 143.3, 143.1, 135.2, 135.0, 134.7, 134.6, 127.6, 127.2, 122.4, 122.1, 120.6, 119.2, 115.2, 114.9, 101.5, 95.0, 57.2, 55.4, 37.3, 37.0, 30.8, 30.6, 30.5, 29.0, 28.9, 28.8, 28.4, 24.14, 24.10, 24.04, 23.45, 23.32, 23.26, 14.32, 14.26, 14.22, 11.01, 10.97, 10.95, 10.85, 10.83, 10.79; MS (APCI$^+$, 20 V), *m*/*z*: 1158 ([M+H]$^+$).

*4.4.5. 5-Bis[3-hydroxy-7-(carbazol-9-yl)-6-(carbazol-9-methyl)-5-oxa-1-heptylamino]-2-phenyl-1,2,3-benzotriazole (**5**).* 5-Amino-2-phenyl-1,2,3-benzotriazole (**1**) (3 g, 0.014 mol) and 1,3-bis(carbazol-9-yl)-2-propanol glycidyl ether (19.2 g, 0.043 mol) were heated in the melt at 160 °C for 24 h. After termination of the reaction (TLC: acetone/*n*-hexane, 7:18 v/v), benzotriazole derivative **5** was purified by column chromatography, using acetone/*n*-hexane (1:4 v/v) as eluent. Recrystallization of the residue from toluene afforded **5** (9.8 g, 62%) as a yellow-green powder, mp: 126–127 °C (toluene); [found: C, 78.42; H, 5.69; N, 10.06. $C_{72}H_{62}N_8O_4$ requires C, 78.38; H, 5.66; N, 10.16%]; R_f (acetone/*n*-hexane, 7:18, v/v) 0.31; ν_{max} (KBr) 3542, 3048, 2927, 2870, 1121 cm^{-1}; δ_H (300 MHz, $CDCl_3$) 8.37–8.28 (m, 2H), 8.09–7.92 (m, 8H), 7.65–7.47 (m, 3H), 7.45–7.07 (m, 25H), 6.61–6.33 (m, 2H), 4.59–4.40 (m, 4H), 4.38–4.20 (m, 6H), 4.43–4.32 (m, 1H), 3.22–3.09 (m, 1H), 2.84–2.66 (m, 4H), 2.45–2.15 (m, 4H), 1.86 (d, *J*=1.9 Hz, 2H); δ_C (75 MHz, $CDCl_3$) 147.5, 146.9, 140.65, 140.51, 140.40, 140.13, 129.6, 128.3, 126.2, 123.1, 120.9, 120.7, 120.1, 119.7, 118.5, 108.84, 108.80, 95.6, 78.47, 78.44, 73.89, 73.76, 68.6, 67.7, 56.3, 54.3, 45.77, 45.67; MS (APCI$^+$, 20 V), *m*/*z*: 1103 ([M+H]$^+$).

*4.4.6. 5-Bis[3-ethoxy-7-(carbazol-9-yl)-6-(carbazol-9-methyl)-5-oxa-1-heptylamino]-2-phenyl-1,2,3-benzotriazole (**6**).* Compound **5** (4.8 g, 4.35 mmol), Na_2SO_4 (0.31 g, 2.18 mmol), and powdered 85% KOH (0.86 g; 13.1 mmol) were refluxed in 40 mL of iodoethane for 24 h. After termination of the reaction (TLC: acetone/*n*-hexane, 7:18 v/v), mixture was cooled to room temperature and filtered off. The organic part was extracted with ethyl acetate distilled water. The organic layer was dried over anhydrous Na_2SO_4, filtered, and solvents were removed. The residue was purified by column chromatography using acetone/*n*-hexane (1:4 v/v) as the eluent to obtain 6 (3.73 g, 74%) as a yellow-green powder; [found: C, 78.79; H, 6.15; N, 9.71. $C_{76}H_{70}N_8O_4$ requires C, 78.73; H, 6.09; N, 9.66%]; R_f (acetone/*n*-hexane, 7:18, v/v) 0.45; ν_{max} (KBr) 3048, 2969, 2867, 1120 cm^{-1}; δ_H (300 MHz, $CDCl_3$) 8.38–8.30 (m, 2H), 8.01 (d, *J*=7.5 Hz, 8H), 7.71–7.60 (m, 1H), 7.59–7.49 (m, 2H), 7.45–7.04 (m, 25H), 6.85–6.75 (m, 1H), 6.69–6.63 (m, 1H), 4.59–4.45 (m, 4H), 4.43–4.20 (m, 6H), 3.07–2.70 (m, 14H), 0.73 (t, *J*=7.0 Hz, 6H); δ_C (75 MHz, $CDCl_3$) 147.2, 147.0, 140.7, 140.47, 140.41, 140.0, 129.5, 128.1, 126.03, 125.99, 123.11, 123.07, 120.56, 120.48, 120.1, 119.50, 119.46, 118.4, 108.9, 93.8, 77.9, 76.15, 76.06, 72.1, 65.69, 65.65, 53.6, 52.9, 46.1, 45.8, 15.6; MS (APCI$^+$, 20 V), *m*/*z*: 1159 ([M+H]$^+$).

*4.4.7. Tetrakis{5-bis[3-hydroxy-7-(carbazol-9-yl)-6-(carbazol-9-methyl)-5-oxa-1-heptylamino]-2-phenyl-1,2,3-benzotriazole-N,C$^{2'}$}(μ-dichloro)diiridium (**7a**).* Iridium trichloride hydrate (0.2 g, 0.67 mmol) and **5** (1.85 g, 1.67 mmol) were dissolved in the mixture of 2-ethoxyethanol (10 mL) and water (5 mL) and refluxed under argon atmosphere for 24 h (TLC: acetone/*n*-hexane, 2:3 v/v). A yellow precipitate was filtered and washed with water and ethanol several times and dried. The μ-chloride-bridged dimer was purified by column chromatography using acetone/*n*-hexane (7:18 and 1:1 v/v) as the eluent to obtain **7a** (1.3 g, 40%) as a yellow powder.

*4.4.8. Tetrakis{5-bis[3-ethoxy-7-(carbazol-9-yl)-6-(carbazol-9-methyl)-5-oxa-1-heptylamino]-2-phenyl-1,2,3-benzotriazole-N,C$^{2'}$}(μ-dichloro)diiridium (**7b**).* Compound **7b** was synthesized by the same procedure as **7a**, except that 0.253 g (0.849 mmol) of iridium trichloride hydrate and 2.46 g (2.12 mmol) of **6** were taken, and dissolved in the mixture of 2-ethoxyethanol (25 mL) and water (5 mL). Purification by column chromatography afforded **7b** (1.7 g, 39%) as a yellow powder.

*4.4.9. Iridium(III)-bis{5-bis[3-hydroxy-7-(carbazol-9-yl)-6-(carbazol-9-methyl)-5-oxa-1-heptylamino]-2-phenyl-1,2,3-benzotriazolato-N,C$^{2'}$}acetylacetonate (**8a**).* Compound **8a** was synthesized by the same procedure as **4** described above, except that μ-chloride-bridged dimer **7a** (1.3 g, 0.267 mmol), 2,4-pentanedione (0.08 g, 0.802 mmol), and Na_2CO_3 (0.28 g, 2.67 mmol) were taken, and dissolved in degassed 2-ethoxyethanol (10 mL) (TLC: acetone/*n*-hexane, 7:18 v/v). The residue was purified by column chromatography using acetone/*n*-hexane (1:4 and 7:18 v/v) as eluent to obtain **8a** (0.79 g, 59%) as an orange powder; [found: C, 71.79; H, 5.14; N, 8.93. $C_{149}H_{129}IrN_{16}O_{10}$ requires C, 71.70; H, 5.21; N, 8.98%]; R_f (acetone/*n*-hexane, 7:18, v/v) 0.15; ν_{max} (KBr) 3400, 3047, 2926, 1698, 1121 cm^{-1}; δ_H (300 MHz, $CDCl_3$) 8.21–7.87 (m, 16H), 7.84–6.03 (m, 62H), 5.03 (s, 1H), 4.72–4.06 (m, 20H), 3.21–2.51 (m, 24H), 1.43 (s, 6H); δ_C (75 MHz, $CDCl_3$) 186.3, 185.9, 150.1, 146.8, 143.2, 140.53, 140.44, 135.2, 134.9, 127.4, 126.24, 126.08, 123.16, 123.14, 122.4, 120.7, 120.4, 119.71, 119.69, 119.2, 115.2, 114.8, 108.83, 108.78, 101.2, 94.9, 78.71, 78.61, 73.86, 73.68, 69.7, 56.4, 54.0, 45.79, 45.70, 31.2, 28.4.

4.4.10. Iridium(III)-bis{5-bis[3-ethoxy-7-(carbazol-9-yl)-6-(carbazol-9-methyl)-5-oxa-1-heptylamino]-2-phenyl-1,2,3-benzotriazolato-

N,C$^{2'}$*}acetylacetonate (**8b**).* Compound **8b** was synthesized by the same procedure as **4**, except that μ-chloride-bridged dimer **7b** (1.6 g, 0.314 mmol), 2,4-pentanedione (0.094 g, 0.943 mmol), and Na_2CO_3 (0.33 g, 3.14 mmol) were taken, dissolved in degassed 2-ethoxyethanol (10 mL) (TLC: acetone/*n*-hexane, 1:4 v/v). The residue was purified by column chromatography using acetone/*n*-hexane (3:22 and 1:4 v/v) as eluent to obtain **8b** (0.87 g, 53%) as an orange powder; [found: C, 72.37; H, 5.64; N, 8.52. $C_{157}H_{145}IrN_{16}O_{10}$ requires C, 72.30; H, 5.60; N, 8.59%]; R_f (acetone/*n*-hexane, 1:4, v/v) 0.17; ν_{max} (KBr) 3047, 2925, 1698, 1120 cm^{-1}; δ_H (300 MHz, $CDCl_3$) 8.20–7.88 (m, 16H), 7.87–6.08 (m, 62H), 5.00 (s, 1H), 4.70–4.03 (m, 20H), 3.19–2.50 (m, 28H), 1.43 (s, 6H), 0.85–0.54 (m, 12H); δ_C (75 MHz, $CDCl_3$) 186.4, 185.2, 150.4, 146.5, 143.3, 140.54, 140.49, 135.1, 134.8, 127.4, 126.14, 126.08, 123.19, 123.14, 122.2, 120.66, 120.60, 120.56, 119.60, 119.56, 119.2, 115.12, 114.95, 108.98, 101.1, 95.1, 78.0, 72.1, 69.6, 65.87, 65.73, 56.1, 53.7, 46.2, 45.9, 30.5, 28.5, 15.65, 15.62.

Acknowledgements

K.K. acknowledges EU Structural Funds project 'Postdoctoral Fellowship Implementation in Lithuania' for funding his postdoctoral fellowship. Financial support from the Research Council of Lithuania and from National Science Council of Taiwan is gratefully acknowledged.

Supplementary data

Supplementary data related to this article can be found online at doi:10.1016/j.tet.2011.01.026. These data include MOL files and InChIKeys of the most important compounds described in this article.

References and notes

1. (a) Baldo, M. A.; O'Brien, D. F.; You, Y.; Shoustikov, A.; Sibley, S.; Thompson, M. E.; Forrest, S. R. *Nature* **1998**, *395*, 151–154; (b) Muller, C. D.; Falcou, A.; Reckefuss, N.; Rojahn, M.; Wiederhirn, V.; Rudati, P.; Frohne, H.; Nuyken, O.; Becker, H.; Meerholz, K. *Nature* **2003**, *421*, 829–833.
2. (a) Adachi, C.; Baldo, M. A.; O'Brien, D. F.; Thompson, M. E.; Forrest, S. R. *J. Appl. Phys.* **2001**, *90*, 5048–5052; (b) Ikai, M.; Tokito, S.; Sakamoto, Y.; Suzuki, T.; Taga, Y. *Appl. Phys. Lett.* **2001**, *79*, 156–159; (c) Lo, S.-C.; Male, N. A. H.; Markham, J. P. J.; Magennis, S. W.; Burn, P. L.; Salata, O. V.; Samuel, I. D. W. *Adv. Mater.* **2002**, *14*, 975–979.
3. Lamansky, S.; Djurovich, P.; Murphy, D.; Abdel-Razzaq, F.; Lee, H.-E.; Adachi, C.; Burrows, P. E.; Forrest, S. R.; Thompson, M. E. *J. Am. Chem. Soc.* **2001**, *123*, 4304–4312.
4. Wang, Y.; Herron, N.; Grushin, V. V.; LeCloux, D.; Petrov, V. *Appl. Phys. Lett.* **2001**, *79*, 449–452.
5. (a) Tsuboyama, A.; Iwawaki, H.; Furugori, M.; Mukaide, T.; Kamatani, J.; Igawa, S.; Moriyama, T.; Miura, S.; Takiguchi, T.; Okada, S.; Hoshino, M.; Ueno, K. *J. Am. Chem. Soc.* **2003**, *125*, 12971–12979; (b) Holmes, R. J.; Forrest, S. R.; Tung, Y. J.; Kwong, R. C.; Brown, J. J.; Garon, S.; Thompson, M. E. *Appl. Phys. Lett.* **2003**, *82*, 2422–2425; (c) Zhou, X.; Qin, D. S.; Pfeiffer, M.; Blochwitz-Nimoth, J.; Werner, A.; Dreschel, J.; Maennig, B.; Leo, K.; Bold, M.; Erk, P.; Hartmann, H. *Appl. Phys. Lett.* **2002**, *81*, 4070–4073.
6. (a) Tokito, S.; Suzuki, M.; Sato, F.; Kamachi, M.; Shirane, K. *Org. Electron.* **2003**, *4*, 105–111; (b) Sandee, A. J.; Williams, C. K.; Evans, N. R.; Davies, J. E.; Boothby, C. E.; Köhler, A.; Friend, R. H.; Holmes, A. B. *J. Am. Chem. Soc.* **2004**, *126*, 7041–7048.
7. Sudhakar, M.; Djurovich, P. I.; Hogen-Esch, T. E.; Thompson, M. E. *J. Am. Chem. Soc.* **2003**, *125*, 7796–7797.
8. (a) Shirota, Y.; Kageyama, H. *Chem. Rev.* **2007**, *107*, 953–1010; (b) Shirota, Y. *J. Mater. Chem.* **2005**, *15*, 75–93; (c) Brunner, K.; van Dijken, A.; Börner, H.; Bastiansen, J. J. A. M.; Kiggen, N. M. M.; Langeveld, B. M. W. *J. Am. Chem. Soc.* **2004**, *126*, 6035–6042; (d) van Dijken, A.; Bastiaansen, J. J. A. M.; Kiggen, N. M. M.; Langeveld, B. M. W.; Rothe, C.; Monkman, A.; Bach, I.; Stössel, P.; Brunner, K. *J. Am. Chem. Soc.* **2004**, *126*, 7718–7727; (e) Tsai, M. H.; Hong, Y. H.; Chang, C. H.; Su, H. C.; Wu, C. C.; Matoliukstyte, A.; Simokaitiene, J.; Grigalevicius, S.; Grazulevicius, J. V.; Hsu, C. P. *Adv. Mater.* **2007**, *19*, 862–866.
9. (a) Ding, J.; Wang, B.; Yue, Z.; Yao, B.; Xie, Z.; Cheng, Y.; Wang, L.; Jing, X.; Wang, F. *Angew. Chem., Int. Ed.* **2009**, *48*, 6664–6666; (b) Wong, W. Y.; Ho, C. L.; Gao, Z. Q.; Mi, B. X.; Chen, C. H.; Cheah, K. W.; Lin, Z. *Angew. Chem., Int. Ed.* **2006**, *45*, 7800–7803; (c) Ding, J.; Gao, J.; Cheng, Y.; Xie, Z.; Wang, L.; Ma, D.; Jing, X.; Wang, F. *Adv. Funct. Mater.* **2006**, *16*, 575–581.
10. Lo, S. C.; Anthopoulos, T. D.; Namdas, E. B.; Burn, P. L.; Sammuel, I. D. W. *Adv. Mater.* **2005**, *17*, 1945–1948.
11. (a) Chen, C.-T. *Chem. Mater.* **2004**, *16*, 4389–4400; (b) Cummings, S. D.; Eisenberg, R. *J. Am. Chem. Soc.* **1996**, *118*, 1949–1960.
12. (a) You, Y.; Park, S. Y. *Dalton Trans.* **2009**, 1267–1282; (b) Wong, W.-Y.; Ho, C.-L. *J. Mater. Chem.* **2009**, *19*, 4457–4482.
13. (a) Beyer, B.; Ulbricht, C.; Escudero, D.; Friebe, C.; Winter, A.; Gonzalez, L.; Schubert, U. S. *Organometallics* **2009**, *28*, 5478–5488; (b) Xia, Z.-Y.; Xiao, X.; Su, J.-H.; Chang, C.-S.; Chen, C. H.; Li, D.-L.; Tian, H. *Synth. Met.* **2009**, *159*, 1782–1785; (c) Tomkute-Luksiene, D.; Malinauskas, T.; Stanisauskaite, A.; Getautis, V.; Kazlauskas, K.; Vitta, P.; Zukauskas, A.; Jursenas, S. *J. Photochem. Photobiol., A* **2008**, *198*, 106–110; (d) Schaefer, T.; Murer, P.; Baudin, G.; Kocher, M.; Maike, F.; Allenbach, S.; Sift, R.; Schmidhalter, B. PCT Int. Appl. WO 2008101842A1, 2008.
14. (a) Xu, M.-L.; Wang, G.-Y.; Zhou, R.; An, Z.-W.; Zhou, Q.; Li, W.-L. *Inorg. Chim. Acta* **2007**, *360*, 3149–3154; (b) Song, Y.-H.; Yeh, S.-J.; Chen, C.-T.; Chi, Y.; Liu, C.-S.; Yu, J.-K.; Hu, Y.-H.; Chou, P.-T.; Peng, S.-M.; Lee, G.-H. *Adv. Funct. Mater.* **2004**, *14*, 1221–1226; (c) Ding, J.; Gao, J.; Fu, Q.; Cheng, Y.; Ma, D.; Wang, L. *Synth. Met.* **2005**, *155*, 539–548.
15. (a) Sinkeviciute, G.; Stanisauskaite, A.; Gaidelis, V.; Jankauskas, V.; Montrimas, E. *Mol. Cryst. Liq. Cryst.* **2007**, *468*, 163–172; (b) Bubniene, G.; Malinauskas, T.; Getautis, V.; Stanisauskaite, A.; Jankauskas, V.; Sidaravicius, J. *Synth. Met.* **2008**, *158*, 670–675.
16. Adams, M. J.; Highfield, J. G.; Kirkbright, G. F. *Anal. Chem.* **1977**, *49*, 1850–1852.
17. Mello, J. C.; Wittmann, H. F.; Friend, R. H. *Adv. Mater.* **1997**, *9*, 230–232.
18. (a) Kirkus, M.; Tsai, M. H.; Grazulevicius, J. V.; Wu, C. C.; Chi, L. C.; Wong, K. T. *Synth. Met.* **2009**, *159*, 729–734; (b) Miyamoto, E.; Yamaguchi, Y.; Yokoyama, M. *Electrophotography* **1989**, *28*, 364–370.